Fouling in heat exchange equipment

Authors: William G. Characklis, Nick Zelver, and Mukesh H. Turakhia.

This is a postprint of a book chapter that originally appeared in Fouling in Heat Exchange Equipment on 1981.

Characklis, W.G., N. Zelver, and M. Turakhia, "Fouling and Heat Transfer," in Chenoweth and Impagliazzo (eds.), Fouling in Heat Exchange Equipment, ASME, HTD, 17:1-15 (1981).

81-009

HTD-Vol. 17 54

Fouling in Heat Exchange Equipment

presented at

THE 20TH ASME/AIChE HEAT TRANSFER CONFERENCE
MILWAUKEE, WISCONSIN
AUGUST 2-5, 1981

sponsored by

THE HEAT TRANSFER EQUIPMENT (k-10) COMMITTEE
OF THE ASME HEAT TRANSFER DIVISION

edited by

JAMES M. CHENOWETH
HEAT TRANSFER RESEARCH, INC.

MIKE IMPAGLIAZZO
STONE & WEBSTER ENGINEERING CORP.

THE AMERICAN SOCIETY OF MECHANICAL ENGINEERS
United Engineering Center 345 East 47th Street New York, N. Y. 10017

FOULING AND HEAT TRANSFER

W. G. Characklis, N. Zelver, and M. Turakhia
College of Engineering
Montana State University
Bozeman, Montana

M. J. Nimmons
D'Appolonia Consulting Engineers, Inc.
Irvine, California

ABSTRACT

Fouling biofilm formation in heat exchange equipment results in a significant energy loss by increasing heat transfer resistance. This paper presents a model for simulating biofilm development and its influence on heat transfer resistance. The model consists of four components: (1) fouling biofilm development, (2) fluid frictional resistance, (3) conductive heat transfer resistance, and (4) convective heat transfer resistance. The model is compared to results obtained in a laboratory heat exchange system and to limited results obtained by others in field tests.

A deposition monitor which operates on the principles of the model is described. The monitor, interfaced to a microcomputer has been developed for industrial use. Computer outputs included fluid frictional resistance, heat transfer resistance, fouling deposit, thermal conductivity and fouling deposit roughness. This information can be used to determine the composition of the fouling deposit without resorting to visual inspection or sampling from the tube.

NOMENCLATURE

A	= wetted surface area	(L^2)
A_I	= inside surface area of biofilm, $2\pi r_I L$	(L^2)
C_p	= specific heat	$(L^2t^{-2}T^{-1})$
f	= friction factor, $2d\Delta p/L\rho_f V_m^2$	(dimensionless)
F_D	= dilution flow rate	(L^3t^{-1})
F_R	= recycle flow rate	(L^3t^{-1})
h	= convective heat transfer coefficient at r_I	$(Mt^{-3}T^{-1})$
k	= fluid thermal conductivity	$(MLt^{-3}T^{-1})$
k_A	= adsorption rate coefficient	(Lt^{-1})
k'_A	= saturation coefficient	(ML^{-2})
k_B	= apparent thermal conductivity of biofilm	$(MLt^{-3}T^{-1})$
k_D	= detachment rate coefficient	(t^{-1})
k'_D	= coefficient	(Lt^2M^{-1})
k_p	= specific biofilm production rate	(t^{-1})
k'_p	= saturation coefficient	(ML^{-3})
k_s	= equivalent sand roughness	(L)
k_{tube}	= thermal conductivity of tube wall material	$(MLt^{-3}T^{-1})$
L	= length of heat exchanger tube	(L)
N	= rate of nutrient consumption by biofilm	$(ML^{-2}t^{-1})$
q_r	= heat flux in -r direction	(Mt^{-3})
q_2	= heat flux at r_2	(Mt^{-3})
Q	= heat transfer rate into the bulk fluid	(ML^2t^{-3})
r	= radial distance	(L)
r_1	= inner radius of tube	(L)
r_2	= outside radius of tube	(L)
r_i	= radial distance to inner thermistor of TWHE	(L)
r_{ii}	= radial distance to outer thermistor of TWHE	(L)
r_I	= radial distance to the biofilm	(L)
R_A	= net rate of transport and adsorption of cells, organic and inorganics to the surface	$(ML^{-2}t^{-1})$
R_B	= net biofilm accumulation rate	(Mt^{-1})
R_D	= rate of detachment of biofilm	$(ML^{-2}t^{-1})$
Re	= Reynolds Number	(dimensionless)
R_f	= fouling factor	(t^3TM^{-1})
R_g	= glucose removal rate	$(ML^{-2}t^{-1})$
s	= limiting nutrient concentration in bulk water	(ML^{-3})
T_1	= temperature at r_1	(T)
T_i	= temperature in TWHE at r_i	(T)
T_{ii}	= temperature in TWHE at r_{ii}	(T)
T_b	= bulk fluid temperature	(T)
Th	= biofilm thickness, r_1-r_I	(L)

T_I = temperature at r_I (T)

U = overall heat transfer coefficient $(Mt^{-3}T^{-1})$

$U^{-1}_{calc} = U^{-1}_{overall}$ calculated by Eq. 10 $(M^{-1}t^3T)$

U^{-1}_{cond} = conductive heat transfer $(M^{-1}t^3T)$

U^{-1}_{conv} = convective heat transfer resistance $(M^{-1}t^3T)$

$U^{-1}_{meas} = U^{-1}_{overall}$ measured in TWHE $(M^{-1}t^3T)$

$U^{-1}_{o} = U^{-1}_{conv}$ in clean tube $(M^{-1}t^3T)$

$U^{-1}_{overall}$ = overall heat transfer resistance $(M^{-1}t^3T)$

v_m = mean fluid velocity (Lt^{-1})

x = biomass concentration in bulk water (ML^{-3})

Y = mass of biofilm produced per unit nutrient mass consumed (dimensionless)

z = length (L)

Δp = pressure drop across length L $(ML^{-1}t^{-2})$

μ = fluid viscosity $(ML^{-1}t^{-1})$

ρ_f = fluid density (ML^{-3})

ρ = biofilm density (ML^{-3})

τ_w = fluid shear stress at biofilm surface $(ML^{-1}t^{-2})$

δ_1 = viscous sublayer thickness (L)

ε = effective height of roughness element (L)

INTRODUCTION

The term fouling refers to the undesirable formation of inorganic and/or organic deposits on surfaces. These deposits can impede the flow of heat across the surface, increase the fluid frictional resistance at the surface, and increase the rate of corrosion at the surface. In each case, energy loss results.

Fouling Deposits

Several types of fouling and their combinations may occur in heat exchangers: (1) crystalline or precipitation fouling, (2) corrosion fouling, (3) particulate fouling, (4) chemical reaction fouling, and (5) biological fouling or biofouling. Biological fouling results from (a) development of an organic film (biofilm) consisting of microorganisms and their products (microbial fouling), (b) deposition and growth of macroorganisms such as barnacles (macrobial fouling), and (c) assorted detritus. Although many different macroorganisms such as barnacles and mussels have been identified in fouling communities, this paper will concentrate on microbial fouling assuming that it always precedes colonization of the surface by macroorganisms. Based on this premise, control of microbial fouling results in control of macrobial fouling.

Biofouling is not limited to microbial activity. The term includes the interaction of the microorganisms and the slime layer with both the chemistry of the solid surface and the bulk fluid. The interaction can enhance some of the more commonly known phenomena such as precipitation or crystallization (scaling) and corrosion. The rate and extent of fouling due to various mechanisms will partially be determined by the physical and transport properties of the resulting fouling films (e.g., thermal conductivity, rheological properties, roughness). There can be no doubt that fouling biofilms that form on condenser surfaces reduce heat transfer and lower plant efficiency. Purkiss (1) observed a decrease of nearly 80% in the performance of a cooling system over a seven week period due to biofouling. Ritter and Suitor (2) measured fouling resistance in six power plant condensers of 240 MW design capacity and estimated the cost of extra fuel for this system due to fouling was $350,000 (1976 dollars).

Relatively little effort has been invested in mechanistic studies relating biofilm development to heat transfer resistance. Kirkpatrick et. al. (3) have developed a mathematical model describing heat transfer and mass transfer for a fluid flowing in a tube in which a biofilm is developing. The Ocean Thermal Energy Conversion (OTEC) program has accumulated field data which is of limited use due to its empirical nature. This paper describes a more fundamental approach focused on the influence of fouling deposits, primarily biofilms, on heat transfer.

Process Description

Development of a systematic understanding of biofouling from field observations has been limited because of the interaction of several contributing rate processes. Mechanistically, fouling biofilm accumulation may be described as the net result of the following:

- Transport of material from the bulk fluid to the surface and adhesion to the surface. Transported materials can be soluble (microbial nutrients and organic salts) or particulate (viable microorganisms, their detritus, or inorganic particles). Fouling begins once these materials adhere to the surface. Suspended particles of sufficient mass may also control films by "scouring" action.
- Microbial reactions within the film. Microbial growth in the biofilm and extracellular polymers produced by the microorganisms contribute to biofilm accumulation and promote adherence of inorganic suspended solids.
- Fluid shear stress at the surface of the film. Such forces can limit the overall extent of the fouling deposit by removing attached material.
- Surface material and roughness. Surface properties can influence micro-mixing near the surface and corrosion processes. Some metal surfaces may release toxic components into the biofilm inhibiting growth and/or attachment. Some metals produce loosely held oxide films under the biofilms. When the oxide film sloughs, the biofilm is also removed.
- Fouling control procedures. Chlorine, the most commonly used chemical, oxidizes biofilm polymers causing disruption and partial removal of biofilm in the fluid shear stress field. Inactivation of a portion of the microbial population also occurs. Altered biofilm "roughness" and decreased viable cell numbers influence "regrowth" rates of the biofilm. Mechanical cleaning physically removes

a portion of the attached film.

Effects of Fouling

Fouling deposits can cause the following deleterious effects in heat exchangers:

- increased fluid frictional resistance
- increased overall heat transfer resistance

Fouling deposits cause increased fluid frictional resistance by decreasing the effective diameter of the heat exchange tube and by increasing the tube roughness. Picologlou et. al. (4) have indicated that biofilms increase frictional resistance primarily by increasing the effective roughness of the tube.

Overall heat transfer resistance is the sum of conductive and convective heat transfer resistances. Convective heat transfer resistance will decrease as fouling progresses due to the increased turbulence resulting from deposit formation. Conductive heat transfer resistance will increase as the insulating fouling deposit accumulates. The relative changes in convective and conductive heat transfer resistance will depend on the following:

- deposit thickness, roughness and thermal conductivity
- fluid flow rate
- radial temperature gradient in the tube

Characklis et. al. (5) have reported the influence of fouling biofilm on conductive and convective heat transfer resistance in tubes in a laboratory system.

MATHEMATICAL SIMULATION OF BIOFOULING IN A CIRCULAR TUBE

A mathematical model simulating fouling biofilm development and its influence on heat transfer will be described. The model may be useful for several purposes including the following (after Himmelblau and Bischoff (6)):

- Economical experimentation - fouling processes can be studied more quickly and economically than possible in the laboratory or field.
- Extrapolation - extreme ranges of operating conditions can be tested which may be impractical otherwise.
- Evaluation of alternative policies - various designs, operating procedures and treatment processes can be tested before decisions are made.
- Design of experiments - the model indicates the variables to be measured and the data that must be provided for useful evaluation procedures.
- Test of sensitivity - the model can indicate which parameters have a significant influence on process behavior.

However, one significant limitation of modelling must be recognized. The success of the model depends heavily on the basic information available. The model is only as accurate as the physical, chemical, and biological data that go into the model.

Model Component 1: Fouling Biofilm Development

Fouling biofilm development is the net result of several physical, chemical and biological processes including the following:

- transport and adsorption of inorganic and organic molecules at the wetted surface
- transport of microbial cells and other particulate material to the wetted surface
- adsorption and microbial adhesion to the surface
- microbial reactions within the biofilm
- detachment of portions of the deposit by fluid shear

Net biofilm accumulation rate, R_B, reflects a combination of all the rate processes above:

$$R_B = R_A A + NAY - R_D A \qquad (1)$$

where R_A = net rate of transport and adsorption of cells, organics and inorganics on the surface $(ML^{-2}t^{-1})$

R_D = rate of detachment of biofilm $(ML^{-2}t^{-1})$

N = rate of nutrient consumption by the biofilm $(ML^{-2}t^{-1})$

A = wetted surface area (L^2)

Y = mass of biofilm produced per unit nutrient mass consumed (dimensionless)

Net rate of transport and adsorption has been described by Fletcher (7) as follows:

$$R_A = k_A x \left(1 - \frac{\rho Th}{k_A'}\right) \qquad (2)$$

where x = biomass concentration in bulk water (ML^{-3})

ρ = biofilm density (ML^{-3})

Th = biofilm thickness (L)

k_A = adsorption rate coefficient (Lt^{-1})

k_A' = saturation coefficient (ML^{-2})

The rate of biofilm production due to nutrient consumption, $N\,Y$, has been experimentally determined by Trulear and Characklis (8) as follows:

$$N\,Y = \frac{k_p \rho Th\, s}{k_p' + s} \qquad (3)$$

where k_p = specific biofilm production rate (t^{-1})

s = limiting nutrient concentration in bulkwater (ML^{-3})

k_p' = saturation coefficient (ML^{-3})

The rate of biofilm detachment due to fluid shear, R_D, has been experimentally determined by Trulear and Characklis (8). An approximate expression can be derived from their data as follows:

$$R_D = \rho Th\, k_D \exp(k_D' \tau_w) \qquad (4)$$

where τ_w = fluid shear stress at the biofilm surface $(ML^{-1}t^{-2})$

k_D = detachment rate coefficient (t^{-1})

k_D' = coefficient (Lt^2M^{-1})

Model Component 2: Fluid Frictional Resistance

Picologlou et. al. (4) have experimentally determined the influence of biofilm on fluid frictional resistance. Friction factor, f, was independent of Reynolds number, Re, for Re > 10,000 when Th exceeded the viscous sublayer thickness, δ_1. However, f was a function of biofilm roughness, ε. Therefore, the following expression describes the dimensionless friction factor (f) in a tube where Th > δ_1 (Davies (9)):

$$f = \left[1.13 - 0.87 \ \ln(\frac{\varepsilon}{2r_I}) \right]^{-2} \qquad (5)$$

where ε = effective height of roughness elements (L)
r_I = (r_1-Th) = effective tube radius (L)
r_1 = tube radius (L)

Friction factor for any thickness and roughness is described by:

$$f = \frac{4r_1}{L} \ \frac{\Delta p}{\rho_f v_m^2} \qquad (6)$$

where Δp = pressure drop across tube length L ($ML^{-1}t^{-2}$)
L = tube length (L)
v_m = mean fluid velocity (Lt^{-1})
ρ_f = fluid density (ML^{-3})

Model Component 3: Conductive Heat Transfer Resistance

The conductive heat transfer resistance due to biofilm, U^{-1}_{cond}, and biofilm thermal conductivity, k_B, were determined by Characklis et. al. (5). Then

$$U^{-1}_{cond} = \frac{r_I}{k_B} \ln\left(\frac{r_1}{r_I}\right) \qquad (7)$$

where k_B = biofilm thermal conductivity ($MLt^{-3}T^{-1}$).

Model Component 4: Convective Heat Transfer Resistance

Colburn (10) proposed a relationship to predict convective heat transfer coefficient from friction factor:

$$h = 0.125 \ f \ C_p^{0.33} \ \mu^{-0.67} \ k^{0.67} \ \rho_f \ v_m \qquad (8)$$

where h = convective heat transfer coefficient ($Mt^{-3}T^{-1}$)
C_p = specific heat of the fluid ($L^2t^{-2}T^{-1}$)
μ = fluid viscosity ($ML^{-1}t^{-1}$)
k = fluid thermal conductivity ($MLt^{-3}T^{-1}$)

Then convective heat transfer resistance, U^{-1}_{conv} = h^{-1}.

Summary

A flow diagram for the model describing biofilm development in a tube and its influence on overall heat transfer resistance is presented in Figure 1. This model has been tested experimentally. Results are presented below.

EXPERIMENTAL SYSTEM

Characklis et. al. (5) have described an experimental reactor system incorporating a thick-walled heat exchanger (TWHE) suitable for observing changes in heat transfer resistance due to fouling (Figure 2). The system consists of a mixing tank (fermenter) and an external tubular recycle loop. The dilution flow rate, F_D, is much smaller than the recycle flow rate, F_R (i.e., $F_D \ll F_R$). Advantages of this system include the following:

1. At the high recycle rates utilized, no longitudinal concentration gradients exist in the tubular recycle loop. The entire system is a continuous stirred tank reactor (CSTR). This simplifies sampling and the mathematics used in data interpretation. This system also minimizes water and chemical consumption.
2. A short mean residence time can be maintained which minimizes biomass activity in the bulk fluid. The microbial activity is restricted to the reactor surfaces.
3. Fluid shear stress and convective heat transfer at the wall are independent of mean residence time in the reactor.

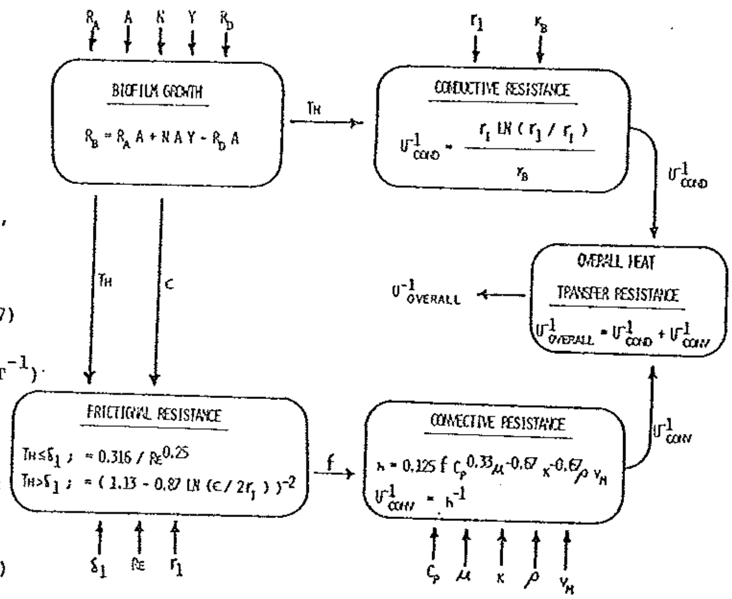

Figure 1. Biofilm development and heat transfer resistance model.

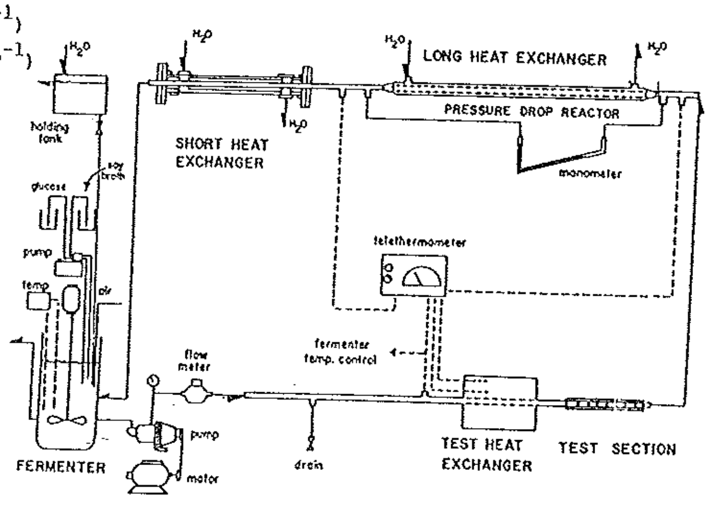

Figure 2. Diagram of experimental system.

Other investigators have used a similar reactor system but have not incorporated heat transfer processes (4). Details of the experimental system are reported elsewhere (5).

Figure 3 is a schematic diagram of the TWHE with a fouled surface being heated at a constant rate. The rate of heat flow from the cylinder to the bulk fluid is expressed as follows:

$$dQ = U\ (2\ \pi\ r_I\ dz)\ (T_i - T_b) \tag{9}$$

where dQ = differential heat transfer rate into the bulk fluid (ML^2t^{-3})

U = overall heat transfer coefficient $(Mt^{-3}T^{-1})$

dz = differential length (L)

T_i = temperature in the tube wall at r_i (T)

T_b = bulk fluid temperature (T)

The overall heat transfer coefficient can be calculated as follows:

$$U = \frac{1}{h} + \frac{r_I\ \ln(r_1/r_I)}{k_B} + \frac{r_I\ \ln(r_i/r_1)}{k_{tube}} \tag{10}$$

where k_{tube} = the thermal conductivity of the tube wall material $(MLt^{-3}T^{-1})$

r_i = radial distance to the thermistor (L)

Overall heat transfer resistance, $U^{-1}_{overall}$, is simply the inverse of U.

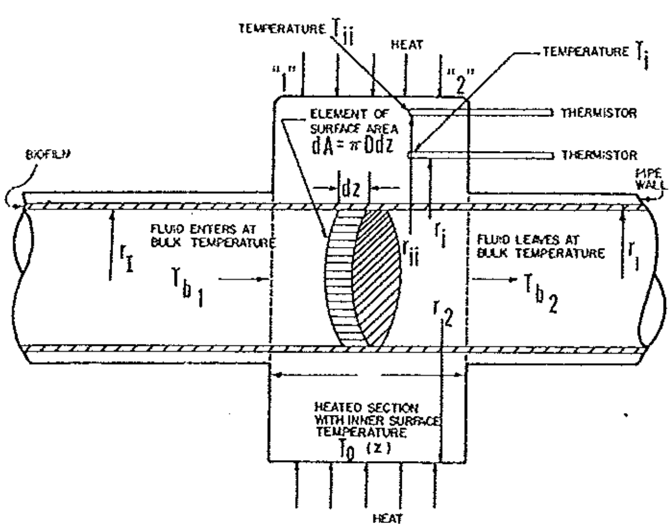

Figure 3. Physical basis for modelling heat transfer in a circular tube with fouling biofilm.

In a clean system (i.e., no biofilm), the second term on the right hand side in Equation 10 goes to zero. As biofilm develops, the overall heat transfer coefficient changes. If the change in T_i and T_b is insignificant with longitudinal distance, L, the integration of Equation 9 over the length of the heated section gives

$$\frac{Q}{A_I} = \left[\frac{1}{h} + \frac{r_I\ \ln(r_1/r_I)}{k_B} + \frac{r_I\ \ln(r_i/r_1)}{k_{tube}}\right]^{-1} \tag{11}$$

where $A_I = 2\pi r_I L$ = inside surface area of biofilm (L^2)

L = length of tube (L)

Overall Heat Transfer Resistance

A steady state heat balance on a differential element of the heated tube (Figure 3) results in the following:

$$\frac{d(rq_r)}{dr} = 0 \tag{12}$$

where $q_r = \frac{dQ}{dA}$ = heat flux in -r direction (Mt^{-3})

Equation 12 can be expressed as follows:

$$\frac{d}{dr}(rk_{tube}\ \frac{dT}{dr}) = 0 \tag{13}$$

Boundary conditions are as follows:

at $r = r_2$; $q_2 = k_{tube}\ \frac{dT}{dr}$

at $r = r_1$; $T = T_1$

where r_2 = outside radius of the tube (L)

q_2 = heat flux at r_2 (Mt^{-3})

The solution of Equation 13 with the boundary conditions yields the following:

$$T - T_1 = \frac{r_2 q_2}{k_{tube}}\ \ln(r/r_1) \tag{14}$$

The tube wall temperature, T_1, is difficult to measure but is related to the bulk fluid temperature as follows:

$$k_{tube}\ \frac{dT}{dr}\Big|_{r=r_1} = U\ (T_1 - T_b) = q_2 \tag{15}$$

Since

$$2\pi r_2 L q_2 = 2\pi r_1 (T_1 - T_b) U$$

Then

$$T_1 = \frac{q_2 r_2}{U\ r_1} + T_b \tag{16}$$

Combining Equations 16 and 14 yields

$$T - T_b = \left[r_2 q_2 \quad \frac{1}{k_{tube}} \quad \ln(r/r_1)\right] + \frac{1}{U\ r_1} \tag{17}$$

By measuring temperatures at two radial positions within the tube wall (r_i and r_{ii}), the effective heat flux (q_2) at the tube outer radius (r_2) can be obtained:

$$q_2 = \frac{k_{tube}(T_{ii} - T_i)}{r_2\ \ln(r_{ii}/r_i)} \tag{18}$$

Having obtained the heat flux, q_2, the overall heat transfer resistance as measured in the TWHE, U^{-1}_{meas}, can be determined by measuring the bulk fluid temperature, T_b, and either T_i or T_{ii}. Solving Equation 17 for the inverse U gives

$$U^{-1}_{meas} = (T_i - T_b) - \frac{r_2 q_2}{k_{tube}} \ln(r_i/r_1) \frac{r_1}{r_2 q_2} \quad (19)$$

Changes in U^{-1}_{meas} may be computed as biofilm develops by monitoring T_i, T_{ii}, and T_b and maintaining a constant heat flux.

This procedure was used to experimentally test the model and describe changes in heat transfer due to biofilm development.

RESULTS

Table 1 presents a summary of experimental conditions and relevant results. The thermal power was maintained constant through all the experiments at approximately 350 watts. The pressure drop (and, therefore, shear stress at the wall) was maintained constant and changes in flow rate were monitored to determine frictional resistance.

Biofilm Development

Biofilm thickness in these experiments was measured in the biofilm test section and increased in a sigmoidal manner as indicated by Figure 4. Others have observed the same characteristic progression (4,11,12). Biofilm thickness within the plateau region ranged from 94-300 μm. The biofilm accumulation occurs at the expense of nutrients. The nutrient (glucose) removal rate also increases with increasing glucose loading rate as evidenced by Figure 5.

Biofilm Properties

Density: Biofilm density ranged from 15-40 mg (dry mass) cm^{-3}. Higher substrate loading have been observed to increase biofilm density (11,12,13) and this trend was observed in this experimentation.

Thermal conductivity: The thermal conductivity of the biofilm, k_B, may be derived by rearranging Equation 10 as follows:

$$k_B = \left[\frac{hk_{tube} - U_{calc}k_{tube} - U_{calc}h\, r_I \ln(r_I/r_1)}{U_{calc}\, h\, k_{tube}\, r_I \ln(r_1/r_I)}\right]^{-1} \quad (20)$$

By measuring biofilm thickness, the overall heat transfer coefficient, and the friction factor, k_B can be determined. Table 2 presents results of k_B determinations and indicates the k_B is not significantly different from the thermal conductivity of water. There was no significant correlation between k_B and biofilm density.

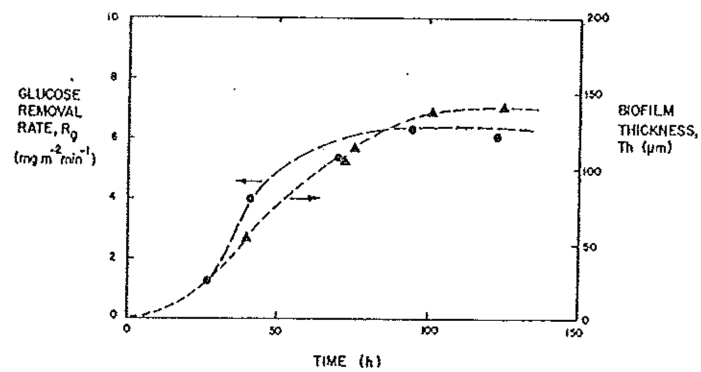

Figure 4. Progression of biofilm thickness and glucose removal rate during a typical experiment.

Frictional Resistance

Frictional resistance is conveniently expressed by a dimensionless friction factor described by Equation 6. In these experiments, v_m was maintained at 80.2 cm s^{-1} (2.6 fps) in the pressure drop section and the change in Δp was monitored across a length of

TABLE 1

Summary of Experimental Results

Experiment	Bulk Temperature T_b	Initial Shear Stress τ_{w_o}	Mean Fluid Velocity v_m	Max. Friction Factor f_{max}	Max. Biofilm Thickness Th_{max}	Biofilm Density ρ	Glucose Loading Rate R_g	Dilution Flow Rate F_D	Biofilm Thermal Conductivity k_B
	°C	N m^{-2}	ms^{-1}	dimensionless	μm	kg m^{-3}	$gm^{-2}min^{-1}$	l min^{-1}	watt m^{-1}°C^{-1}
1	31.9	2.20	.809	0.067	245	39.9	682.	0.474	0.70
2	31.5	2.28	.807	0.092	94	18.3	68.	0.474	0.71
3	31.5	2.28	.805	0.037	94	14.4	34.	0.474	--
6	28.3	2.28	.807	0.208	141	16.2	68.	0.474	0.68
7	26.7	2.30	.807	0.154	259	28.0	171.	0.474	0.52
8	26.7	2.28	.808	0.212	232	23.6	68.	0.474	0.70
9	28.3	2.28	.807	0.202	128	24.0	68.	0.474	0.58
10	31.5	2.28	.808	0.030	0	--	0	0.474	no biofilm

329 cm. After an initial period of no change, f increased with increasing biofilm thickness (Figure 6). The cause for increased f has been discussed in detail elsewhere (4). f increases more rapidly at higher glucose loading rates. The increase in f is sometimes followed by a dramatic decrease observable in experiments with high glucose loading rate (Figure 7).

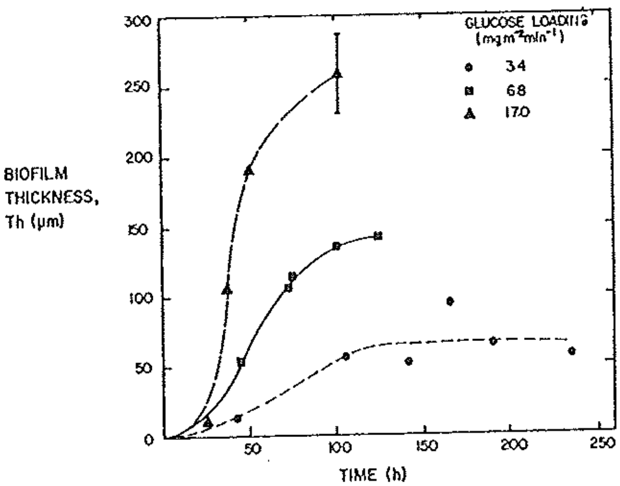

Figure 5. Influence of glucose loading rate on fouling biofilm development.

Overall Heat Transfer Resistance

Measured overall heat transfer resistance is given by Equation 19. U^{-1}_{meas} was determined from measurements of T_i, T_b and power input. Power input was maintained at 350 watts for all experiments so heat flux on the outside wall was approximately 4.86 kW m^{-2}.

Observed heat transfer resistance decreased (3-9% of initial value) during the early stages of all but two of the experiments. Subsequent to this period, heat transfer resistance increased substantially with biofilm thickenss as indicated in Figure 8. Heat transfer resistance increased more rapidly in experiments with higher glucose loading rates and exhibited the same dramatic decrease as observed with friction factor in those experiments (Figure 9).

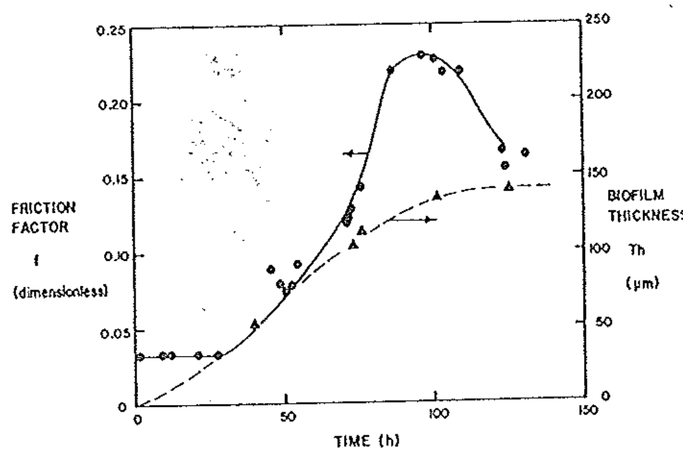

Figure 6. Progression of biofilm thickness and friction factor during a typical experiment.

DISCUSSION

These experiments were conducted to determine the influence of biofilm formation on heat transfer resistance. Accordingly, a laboratory apparatus was

TABLE 2

Thermal Conductivity of Biofilms

Experiment	Biofilm Thermal Conductivity, k_B (watt m^{-1} °C^{-1})	Bulk Temperature, T_b (°C)
1	0.7 ± 0.4 (3)	31.9 ± 0.5
2	0.7 ± 0.1 (3)	31.50 ± 0.03
6	0.7 ± 0.2 (5)	28.30 ± 0.03
7	0.5 ± 0.2 (3)	26.7 ± 0.03
8	0.7 ± 0.4 (5)	26.70 ± 0.03
9	0.6 ± 0.1 (5)	28.30 ± 0.03
Grand Mean	0.6 ± 0.2 (24)	
Water*	0.61 0.62	26.7 32.2

* From Weast (11)

constructed to simulate biofilm development in a heated tube as might occur in a condenser or heat exchanger.

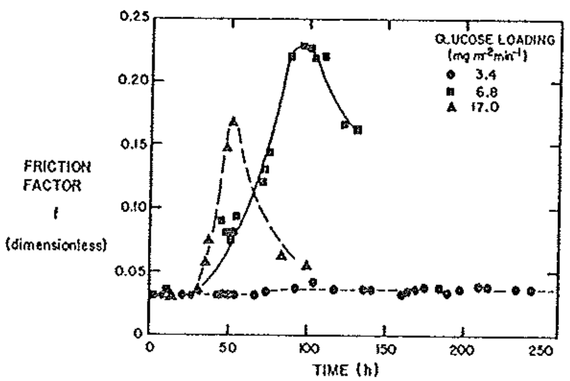

Figure 7. Influence of glucose loading rate on friction factor increase.

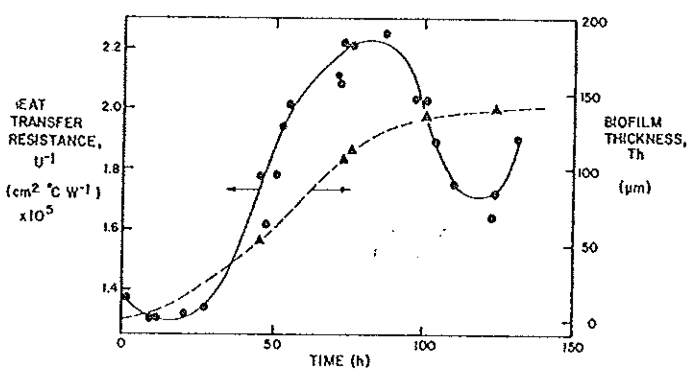

Figure 8. Progression of biofilm thickness and heat transfer resistance during a typical experiment.

Limitations of the Reported Results

Several fundamental limitations must be considered when attempting to apply these results to biofouling in condensers or heat exchangers:

1. A soluble substrate (glucose) was used as the sole energy source for microbial growth. Cooling waters contain more complex carbon and energy sources. Consequently, microbial growth processes will probably be slower in real systems. Furthermore, the carbon and energy sources will be site-specific.

2. The microbial inoculum for all laboratory experiments was composed of a variety of microbial species. Use of a single substrate, however, essentially precludes the maintenance of a stable, mixed population. Therefore, as an experiment progressed, the microbial population was probably dominated by a very few species which could compete better for the available nutrients under the imposed experimental conditions. Microbial population diversity in cooling waters will be site-specific.

3. The feed water in this research contained less than 1 mg/l inert suspended solids. Suspended solids in cooling waters can significantly influence deposit accumulation in a heated tube.

4. Within the experimental apparatus, a stainless steel tube was used for pressure drop measurement and biofilm samples while the test heat exchanger was aluminum.

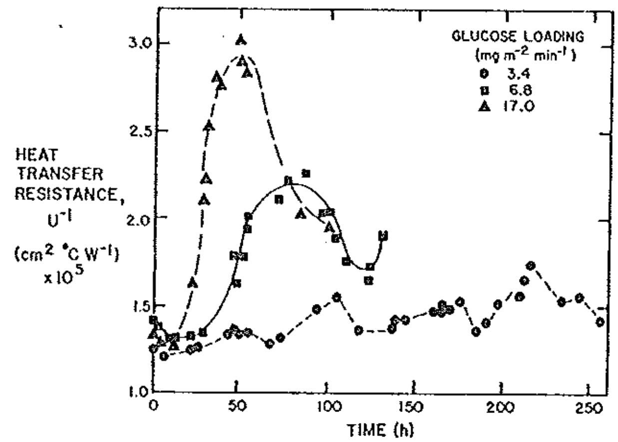

Figure 9. Influence of glucose loading rate on heat transfer resistance during a typical experiment.

Heat Transfer Resistance

Overall heat transfer resistance can be considered the sum of the convective heat transfer resistance and the conductive heat transfer resistance as suggested by Equation 10 which gives

$$\underbrace{U^{-1}_{overall}}_{\text{overall heat transfer resistance}} = \underbrace{\frac{1}{h}}_{\text{convective heat transfer resistance}} + \underbrace{\frac{r_I \ln(r_1/r_I)}{k_B}}_{\text{conductive heat transfer resistance in the biofilm}}$$

$$+ \underbrace{\frac{r_I \ln(r_i/r_1)}{k_{tube}}}_{\text{conductive heat transfer resistance in the tube}} \qquad (10)$$

In these experiments, $U^{-1}_{overall}$ was measured (U^{-1}_{meas}) directly from temperature measurements within the thick-walled heat exchanger (Equation 19). However, friction factor and biofilm thickness measurements permit calculation of $U^{-1}_{overall}$ from Equation 10 and

$r_I = r_1$ - Th and $k_B = k_{water}$.

Figures 10, 11, and 12 compare U^{-1}_{meas} and U^{-1}_{calc} from three experiments at different substrate loadings. In most cases, U^{-1}_{calc} is a good estimate of U^{-1}_{meas}. There were notable exceptions:

1. During the initial or induction period of the experiment when friction factor remains constant.

2. Following a dramatic decrease in U^{-1}_{meas} and f when a mature biofilm is present.

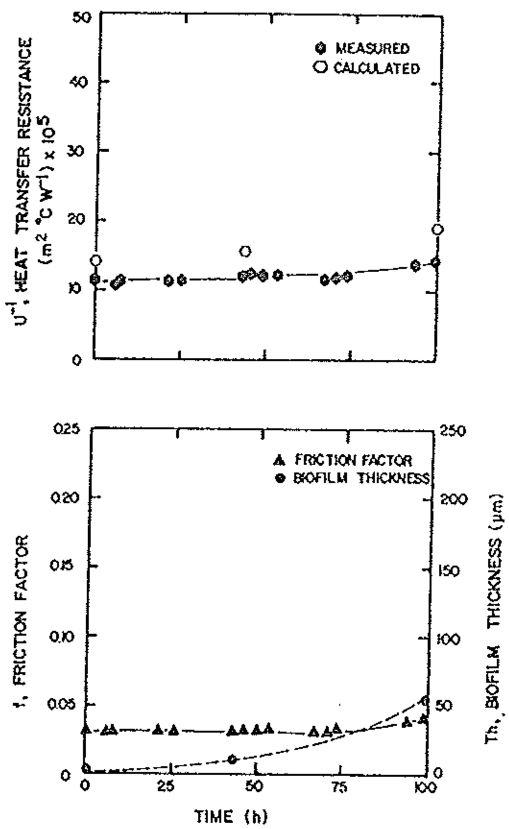

Figure 10. Comparison of measured and calculated values for heat transfer resistance at glucose loading rate = 3.4 mg m^{-2} min^{-1}

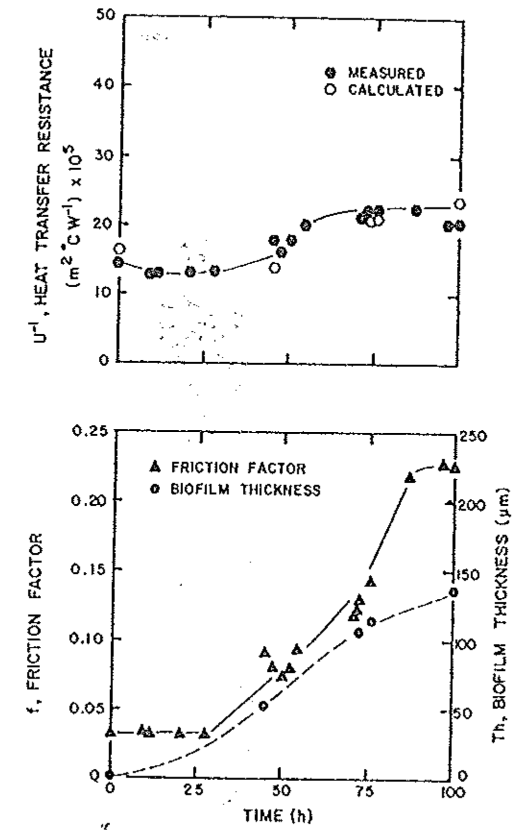

Figure 11. Comparison of measured and calculated values for heat transfer resistance at glucose loading rate = 6.8 mg m^{-2} min^{-1}.

Induction Period. During the induction period, biofilm thickness is small and the "hydraulic" roughness it effects cannot be detected by pressure drop measurements. Picologlou et. al. (4) indicate that no measurable change in frictional resistance will occur until the biofilm thickness approaches the viscous sublayer thickness. In these experiments, the calculated viscous sublayer thickness was 44 μm. Figure 13 indicates that the critical biofilm thickness (Th_c) for changing frictional resistance ranged from 30-60 μm. Other data (12) presented in Figure 14 further demonstrate the critical biofilm thickness concept.

When biofilm thickness, Th, is less than the viscous sublayer thickness, U^{-1}_{calc} and U^{-1}_{meas} are significantly different. Figure 15 compares U^{-1}_{calc} and U^{-1}_{meas} during the initial period of a typical experiment. Time smoothed biofilm thickness values have been used for U^{-1}_{calc}. The discrepancy between U^{-1}_{calc} and U^{-1}_{meas} is large prior to observing a friction factor increase. Subsequent to a friction factor increase, U^{-1}_{calc} and U^{-1}_{meas} are essentially equal. One possible explanation is that roughness caused by the biofilm (when Th < Th_c) increases convective heat transfer before the biofilm causes a change in friction factor. Further evidence for this effect is the observed decrease in U^{-1}_{meas} in the early stages of the experiment. Even if there were no increase in conductive resistance due to biofilm development, U^{-1}_{meas} should remain constant until friction factor changes if the biofilm surface were smooth.

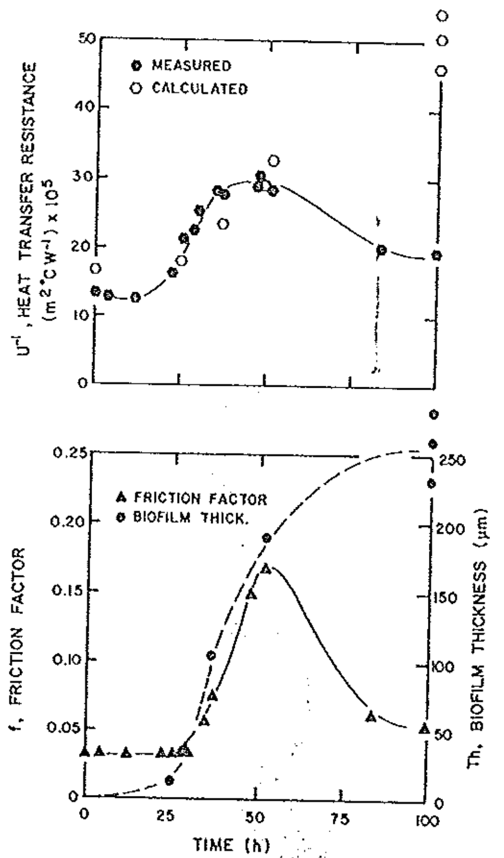

Figure 12. Comparison of measured and calculated values for heat transfer resistance at glucose loading rate = 17.0 mg m^{-2} min^{-1}.

Mature biofilms. In several experiments, a dramatic decrease in heat transfer resistance and frictional resistance were observed without a decrease in biofilm thickness (Figure 12). Possible explanations for this behavior include the following:

1. Tube wall temperature increased causing changes in biofilm properties which affect $U^{-1}_{overall}$ and f. In experiment 7, wall temperature was initially 34.7°C and increased to 44.0°C when $U^{-1}_{overall}$ was at its maximum. The increase in wall temperature may cause changes in the microbial population within the biofilm and/or the chemical properties of the biofilm.

2. Events occurring in the aluminum heat exchanger were not duplicated in the stainless steel sections in which friction factor was measured and biofilm thickness determined.

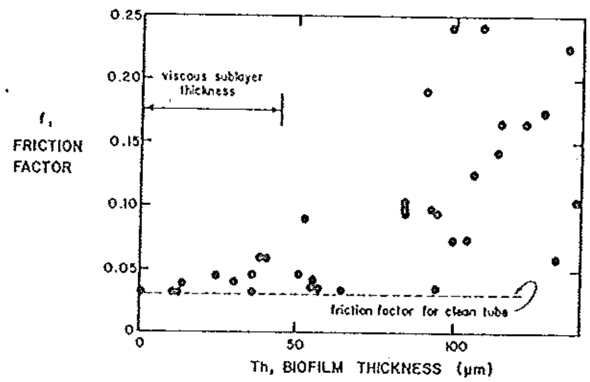

Figure 13. Influence of biofilm thickness on friction factor indicating negligible change in f when Th < viscous sublayer thickness. Data collected from all experiments are plotted (glucose loading rate varied from 3.4 - 17.0 mg m^{-2} min^{-1}).

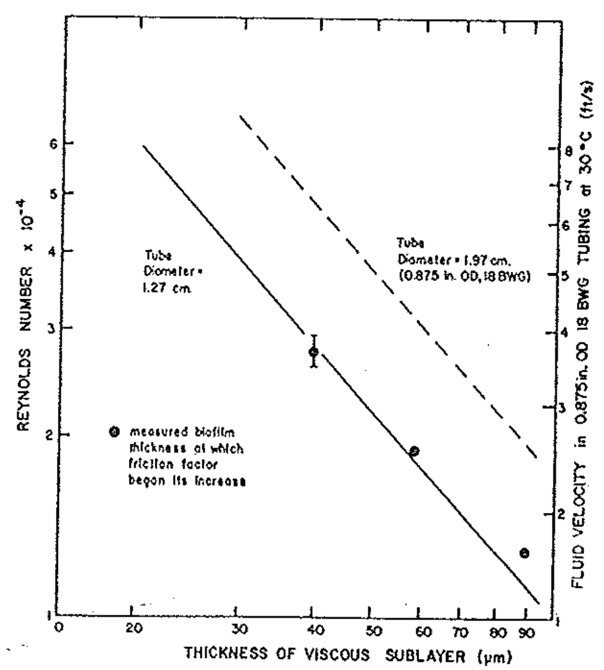

Figure 14. Influence of Reynolds Number on thickness of the viscous sublayer. Circles indicate predicted viscous sublayer thickness based on measured biofilm thickness.

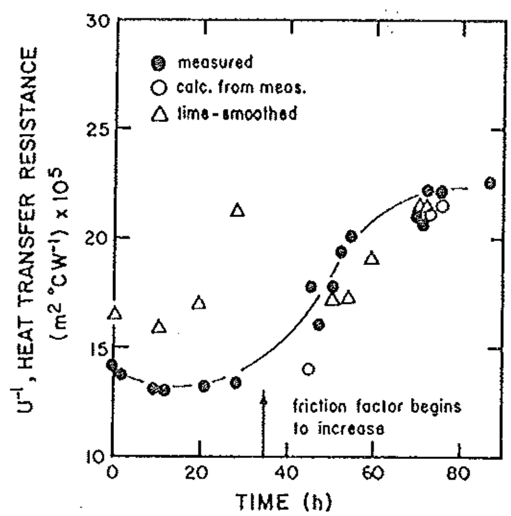

Figure 15. Comparison between measured and calculated heat transfer resistance indicating large discrepancy during period when friction factor remains constant (biofilm thickness < viscous sublayer thickness).

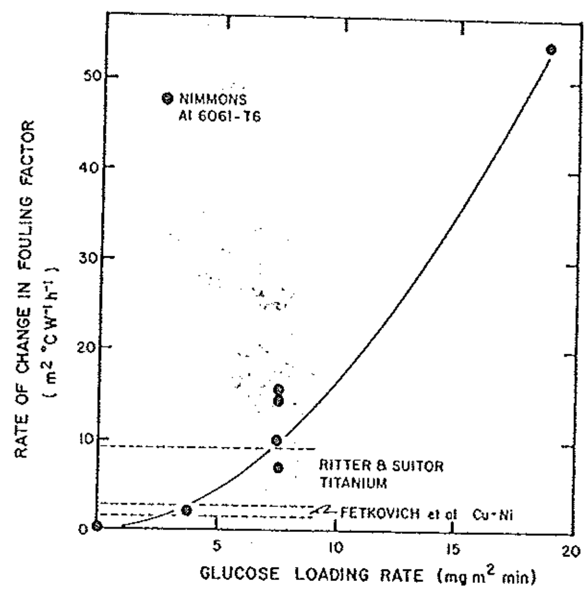

Figure 16. Influence of glucose loading rate on rate of increase in fouling factor (R_f). Ritter and Suitor (2) data obtained at v_m = 0.6-1.2 m s^{-1} and T_1 = 26-38°C. Fetkovich et. al. (14) data obtained at v_m = 0.9-1.8 m s^{-1} and T_1 = 21°C. Nimmons (18) data obtained at v_m = 0.8 m s^{-1} and T_1 = 39.45°C.

Influence of Substrate Loading

Other investigators have measured the influence of biofilms on heat transfer resistance. The data are generally expressed in terms of the fouling factor, R_f, which is defined as follows:

$$R_f = U^{-1}_{overall} - U^{-1}_{o} \tag{21}$$

where U_o = initial convective heat transfer coefficient $(Mt^{-3}T^{-1})$

R_f = fouling factor $(t^3T\ M^{-1})$

The data from two field investigations (2,14) were chosen for comparison to R_f values calculated from data presented in this paper. Both studies were accomplished in seawater where microbial nutrient concentrations are low and biofilm development occurs at a low rate. Stumm and Morgan (15) indicated that organic carbon concentration in the oceans ranges from 0.5-1.2 mg carbon l^{-1}. Higher concentrations would be measured in estuarine waters. Organic carbon concentrations entering the experimental system ranged from 4-80 mg/l resulting in organic carbon loadings in the range of 2.7-55 mg $m^{-2}min^{-1}$. Glucose carbon represented approximately one half the organic carbon entering the system.

Figure 16 clearly indicates the significant influences of substrate loading on the rate of increase in heat transfer resistance. At very high loadings, the rate is expected to either level off or decrease.

FOULING IN THE PLANT ENVIRONMENT

Fouling treatment and control depends on the type of deposit (Table 3) and, in some cases, treatment for one condition may be antagonistic to control of another. Therefore, the composition of a fouling deposit determines the proper treatment schedule. Traditionally, water quality parameters (chemical analysis, selective ion electrodes and bacterial counts) have been used to predict fouling potential and determine treatment. However, these parameters define conditions in the bulk water which generally are significantly different from surface conditions where the problem exists. More recently, fouling monitors have been developed which indicate the effects of a fouling deposit on frictional resistance and heat transfer resistance. These measurements, however, yield no information regarding the composition of the deposit. Our goal is to develop a comprehensive fouling monitor system to determine the rate and extent of fouling and the type of fouling deposit so that appropriate treatment can be applied.

Fouling deposits are rarely homogeneous. Generally, the fouling deposit is a combination of biofilm, scale and corrosion products. The degree to which each type of deposit contributes to fouling is dependent on such factors as water quality changes, plant upsets, operation schedules, and water treatment program. Basic differences in the effects of scale and biofilms on thermohydrodynamic measurements, in conjunction with water quality measurements, can provide useful insight to distinguishing between scale and biofilm, particularly once a history of heat exchanger performance has been established.

TABLE 3

Fouling Treatment and Control

	Scaling	Biofouling
External Treatment	Softening Ion exchange	
Internal Treatment	pH control Softening Acid feed Side stream treatment Flocculants Dispersants Surfactants Chelants	pH control Oxidizing biocides - chlorine - ozone - bromine - hydrogen-peroxide Non-oxidizing biocides - chlorinated phenolics - organo-tin ammonium salts - surfactants
Removal	Mechanical cleaning Acid treatment	Mechanical cleaning Oxidizing biocides

A Fouling Monitor

The fouling monitor system used in our research (Figure 17) consists of two major components:

1. A tube contains ports for pressure drop measurement and a heat transfer section consisting of an electrically heated aluminum block which is clamped around the tube and contains two temperature probes. The tube can be selected to match the alloy of concern. The system also includes a flow meter and a bulk water temperature probe.

2. A microcomputer calculates frictional resistance, convective and conductive heat transfer resistance, and overall heat transfer resistance. The microcomputer also controls flow rate in the tube and controls heat flux to the tube. Output from the microcomputer includes a television monitor displaying all pertinent measurements and calculations and a cassette recorder for storing historical data.

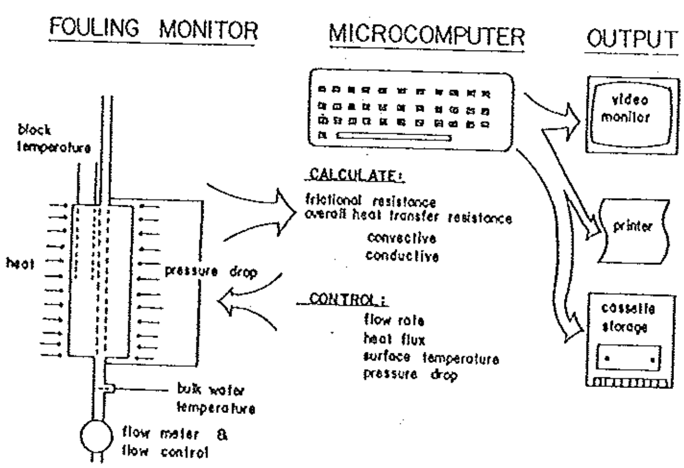

Figure 17. Fouling monitoring system.

Frictional resistance is determined from pressure drop and flow measurements in the tubular section; a detailed discussion of frictional resistance due to biofilms and friction factor calculation is given by Picologlou, et. al. (4). Figure 18 shows the increase of pressure drop with time due to biofilm accumulation in a constant flow-rate laboratory experiment. Frictional resistance due to fouling has been observed in the field. Figure 19 shows a 30% increase in friction factor during a 15 day period at a power plant location.

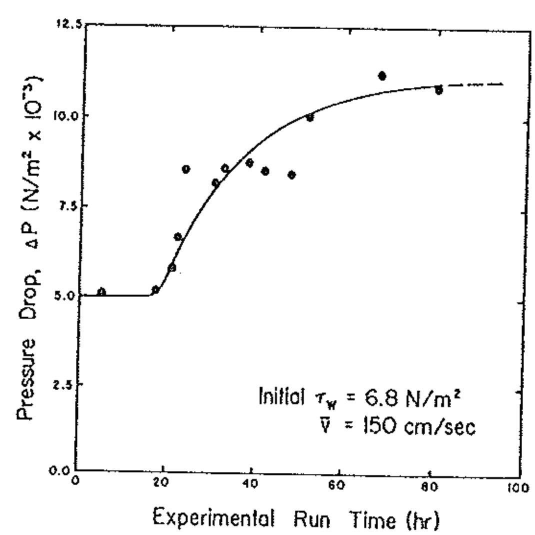

Figure 18. Change in pressure drop with time due to biofilm accumulation in a constant flow rate laboratory experiment.

Picologlou, et. al. (4) have shown constriction of a tube to be an insignificant cause of frictional resistance resulting from biofilm formation. Figure

20 indicates: (1) the increase in pressure drop and biofilm thickness with time during a laboratory experiment; and (2) the increase in pressure drop as calculated from the Blasius equation for a smooth tube for a decrease in radius equal to the measured biofilm thickness. In contrast, constriction of tubing by scale deposits has been shown to be substantial (Cowan and Weintritt, (16)).

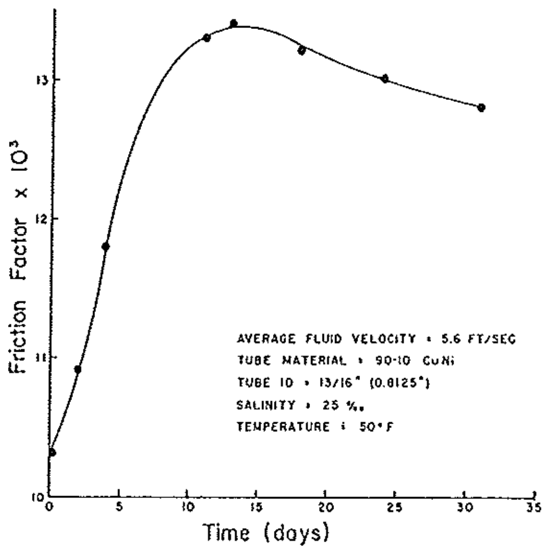

Figure 19. Increase in frictional resistance due to fouling in the field (17).

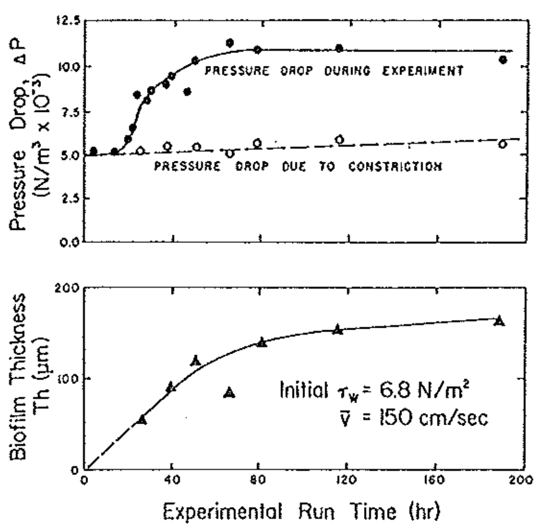

Figure 20. Measured pressure drop compared to calculated pressure drop due to decrease in tube radius equivalent to biofilm thickness.

Figure 21 illustrates the pronounced effective roughness of a biofilm as indicated by calculated equivalent sand roughness. Equivalent sand roughness can be significantly greater than biofilm thickness. The frictional resistance due to the compliant roughness of a biofilm cannot be completely explained by the hydrodynamic principles of rigid rough surfaces. Scale, a relatively rigid rough surface, is hypothesized to affect frictional resistance differently than biofilms; experiments to test this hypothesis are currently being conducted.

Overall heat transfer resistance is calculated from measurements of bulk water temperature and temperature in the aluminum block. Convective heat transfer resistance is dependent on turbulence and is calculated from the friction factor and the properties of the water. Conductive heat transfer resistance is simply determined as the difference in overall and convective heat transfer resistance.

A comparison of thermal conductivities for biofilm and scale is shown in Table 4. The greater thermal conductivities for the more common scale types suggests a method for distinguishing between scale and biofilm. Figure 22 illustrates how this difference in thermal conductivity affects conductive heat transfer resistance.

The relative contribution of convective resistance and conductive resistance to overall heat transfer due to a biofilm deposit in a laboratory experiment is shown in Figure 23. The low convective resistance is due to the pronounced effective roughness of the biofilm causing increased turbulence. Experiments are now being conducted to determine the effective roughness of scale deposits and, unless scale shows an unexpected high effective roughness, conductive resistance will be greater for scale than for biofilms.

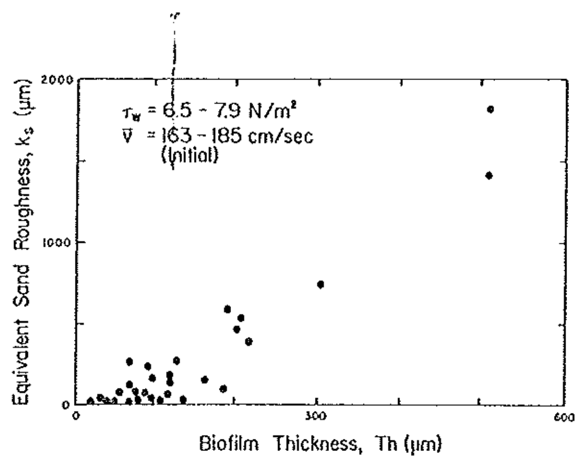

Figure 21. Change in calculated equivalent sand roughness with biofilm thickness for all experiments conducted at constant pressure drop.

TABLE 4

Thermal Conductivities of Scales and Biofilm

Scale[6]	Thermal Conductivity (watt M^{-1} °C^{-1})
Calcium Carbonate	2.26 - 2.93
Calcium Sulfate	2.31
Calcium Phosphate	2.60
Magnesium Phosphate	2.16
Magnetic Iron Oxide	2.88
Analcite	1.27
Biofilm[4,5]	
(Water)	0.63

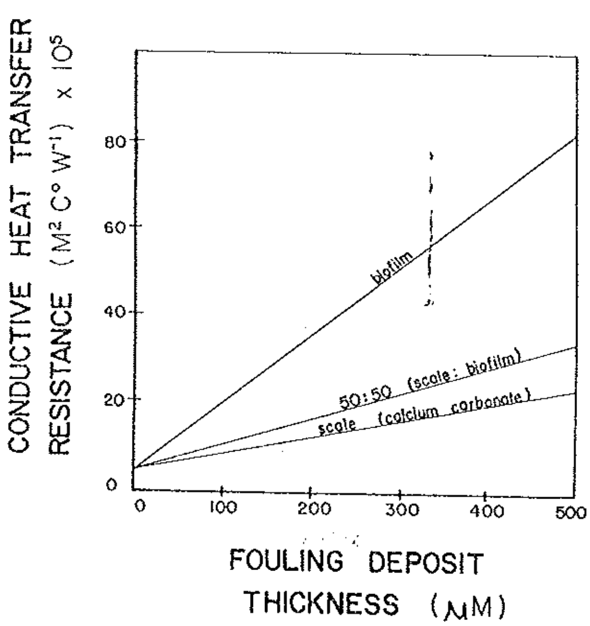

Figure 22. Conductive heat transfer resistance for biofilm and scale as a function of fouling deposit thickness.

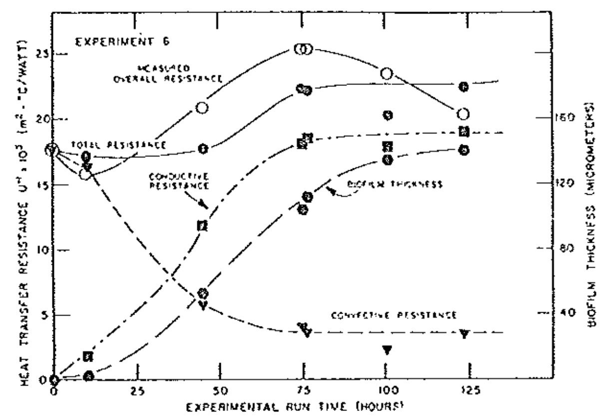

Figure 23. Change in total heat transfer resistance, conductive resistance and convective resistance as a result of biofilm accumulation.

SUMMARY

A mathematical model has been presented which describes biofilm development and its influence on heat transfer in a heated tube. Experimental results from a laboratory heat exchanger indicate satisfactory agreement between the model and the actual process. However, agreement was poor when biofilm thickness did not exceed the viscous boundary layer thickness. A deposition monitor with an interactive microcomputer has been described. The monitoring system has been developed for industrial use to provide continuous output of fluid frictional resistance, heat transfer resistance, fouling deposit thermal conductivity and fouling deposit roughness.

ACKNOWLEDGEMENTS

The authors gratefully acknowledge the National Science Foundation (CPE-8017439), Office of Naval Research (N00014-80-0475), and Calgon Corporation for partial financial support and S. Vehnekamp and M. Mace for manuscript preparation.

REFERENCES

1 Purkiss, B.E., Biotechnology of Industrial Water Conservation, M&B Monographs, Mills and Boon, London, 1972.

2 Ritter, R.B. and Suitor, J.W., "Fouling Research on Copper and Its Alloys - Seawater Studies," HTRI Progress Report, INCRA Project No. 214A, April 1976.

3 Kirkpatrick, J.P., McIntire, L.V. and Characklis, W.G., "Mass and Heat Transfer in a Circular Tube with Biofouling," Water Research, vol. 14, 1980, p.117.

4 Picologlou, B.F., Zelver, N. and Characklis, W.G., "Biofilm Growth and Hydraulic Performance," J. Hyd. Div., Proc. ASCE, vol. 106, no. HY5, 1980, p. 733.

5 Characklis, W.G., Nimmons, M.J., and Picologlou, B.F., "Biofilm Development and Heat Transfer," accepted by Heat Transfer Engineering, 1981.

6 Himmelblau, D.M., and Bischoff, K.B., Process Analysis and Simulation, John Wiley and Sons, New York, 1968.

7 Fletcher, M., "The Effect of Culture Concentration and Age, Time, and Temperature on Bacterial Attachment to Polystyrene," Canadian Journal of Microbiology, vol. 23, 1977, pp. 1-6.

8 Trulear, M.G., Characklis, W.G., "Dynamics of Biofilm Processes," accepted for publication, Journal Water Pollution Control Federation, 1981.

9 Davies, J.T., Turbulence Phenomena, Academic Press, New York, 1972.

10 Colburn, A.P., "A Method of Correlating Forced Convection Heat Transfer Data and a Comparison with Fluid Friction," Trans. A.I.Ch.E., vol. 29, 1933, p. 174.

11 Trulear, M.G. and Characklis, W.G., "Dynamics of Biofilm Processes," Proceedings of 34th Ind. Waste Conf., Purdue Univ. Ann Arbor Science, 1980, p. 838.

12 Characklis, W.G., "Biofouling Film Development and Destruction," Electric Power Res. Inst., RP902-1, 1980.

13 Zelver, N., Biofilm Development and Associated Energy Losses in Water Conduits, M.S. Thesis, Rice University, Houston, TX, 1979, 180 p.

14 Fetkovich, J.G., Grannemann, G.N., Mahalingam, L.M. and Meier, D.L., "Measurements of Biofouling in OTEC Heat Exchangers," Proceedings of 5th OTEC Conf., Miami, Feb. 1978.

15 Stumm, W. and Morgan, J.J., Aquatic Chemistry, Wiley-Interscience, New York, 1970.

16 Cowan, J.C. and Weintritt, D.J., Water-Formed Scale Deposits, Gulf Publishing Company, Houston, TX, 1976.

17 Dehart, R., Personal Communication, 1979.

18 Nimmons, M.J., Heat Transfer Effects in Turbulent Flow Due to Biofilm Development, M.S. Thesis, Rice University, Houston, TX, 1979, 120 p.